Research Article | Vol. 14, No. 8 / 1 Aug 2024 / Optical Materials Express 1972

Optical Materials EXPRESS

Design of near-perfect absorptance in few-layer WSe_2 via cooperative enhancement mechanisms

Ekin Gunes Ozaktas,[1] Sreyas Chintapalli,[1] Serene Kamal,[1] and Susanna M. Thon[1,2,*]

[1]Department of Electrical and Computer Engineering, Johns Hopkins University, USA
[2]Department of Materials Science and Engineering, Johns Hopkins University, USA
[*]susanna.thon@jhu.edu

Abstract: Two-dimensional transition metal dichalcogenides are of growing interest for flexible optoelectronics and power applications, due to their tunable optical properties, lightweight nature, and mechanical pliability. However, their thin nature inherently limits their optical absorption and, therefore, efficiency. Here, we propose a few-layer WSe_2 optoelectronic device that achieves near perfect absorption through a combination of optical effects. The WSe_2 can be scalably grown below an Al_2O_3 superstrate. Our device includes a corrugated back reflector, modeled as a plasmonic nanowire array. We investigate the entire range of widths of the corrugations in the back reflector, including the edge cases of a simple back mirror (width equal to period) and a Fabry-Perot cavity (zero width). We demonstrate the zero-mode enhancement arising from the back reflector, the weakly coupled enhancement arising from the Fabry-Perot cavity, and the strongly coupled enhancement arising from the localized surface plasmon resonance of the nanowires, explain the physical nature of the spectral peaks, and theoretically model the hybridization of these phenomena using a coupled oscillator model. Our champion device exhibits 82% peak absorptance in the WSe_2 alone, 92% in the WSe_2 plus nanowires, and 98% total absorptance. Thus, we achieve a near-perfect absorber in which most of the absorption is in the few-layer WSe_2, with a desirable device framework for integration with scalable growth of the WSe_2, thereby making our designs applicable to a range of practical optoelectronic devices.

1. Introduction

Two-dimensional materials such as transition metal dichalcogenides (TMDs) have gained increasing popularity in recent years due to their desirable properties, among them the presence of a direct bandgap at monolayer thicknesses, removing the necessity for phonon-assisted exciton formation [1]. Further, the atomically thin nature of these materials makes them excellent candidates for ultrathin, flexible and wearable power sources and electronics [2–5]. However, the use of thin materials has the inherent drawback that despite the desirable band structure, the capability of a material to absorb light is significantly impeded by its thinness. To increase absorption in materials of sub-wavelength thickness, a variety of optical enhancement methods have been proposed, including the use of back reflectors, Fabry-Perot (FP) cavities, and dielectric or plasmonic nanostructures.

Pioneering works investigating the optical behavior of a sub-wavelength lossy film atop a real metal highlighted the potential of such structures for high optical absorption even when the absorbing film is only a few nanometers thick [6–8]. This absorption is due to phase changes arising not only from optical path differences in propagation, but more importantly from the interfaces, where the phase change is not 0 or π as in the case of lossless dielectrics or a perfect electrical conductor (PEC) [6]. This results in the so-called “zero-mode", i.e. the lowest order mode arising from the expansion of the quasinormal modes of the structure [7]. Both this effect and other FP cavity based approaches utilize interference-based light trapping in planar devices, with the aim of increasing absorption in one of the layers or in the device as a whole [9–15].

#530780 https://doi.org/10.1364/OME.530780
Journal © 2024 Received 24 May 2024; revised 1 Jul 2024; accepted 6 Jul 2024; published 17 Jul 2024

Optical Materials EXPRESS

The simplest such device in the context of TMDs enhances the absorption of a monolayer or few-layer TMD via a back mirror, often spaced some distance away from the TMD to ensure maximum constructive interference [16–18]. Moreover, the use of plasmonic nanostructures with surface plasmon polariton (SPP) or localized surface plasmonic resonances (LSPRs) to enhance absorption in thin layers, such as TMDs, has also been widely studied [19–31]. These approaches alone or in combination typically result in coupling between the various resonant modes involved — FP, LSPR, or excitonic modes arising from the absorber. There are various coupling regimes that can arise. Weak coupling is the enhancement of emission in which the presence of a cavity increases the local density of states and enhances the strength of an emitter by the Purcell factor. In this regime, the decay rate of each mode is greater than the rate of energy exchange between the modes, resulting in weak coupling. On the other hand, if the relationship between the rates is reversed, it is possible to observe several Rabi oscillations before the modes decay. This is referred to as the strong coupling regime and results in Rabi splitting in the frequency domain and thus the formation of new energetic eigenstates of the system, a phenomenon also termed "anti-crossing" [32,33]. The resulting hybridized modes are often referred to as polaritons, with the specific nature depending on which modes have taken part in the hybridization.

In the present work, we numerically and analytically investigate the strongly coupled excitonic, LSPR, and surface lattice resonance (SLR) modes in the presence of a back reflector and FP cavity. The spectral range of interest is approximately 400 − 1500 nm (0.8 − 3.0 eV), spanning the visible and near infrared (NIR) regions of the spectrum. Our goal is to design a near-perfect absorbing few-layer TMD device and investigate the coupling phenomena, under the constraint that the WSe_2 be growable via chemical vapor deposition (CVD). In Section 2, we demonstrate weakly coupled enhancement arising from a planar Fabry-Perot cavity. We build on this structure in Section 3, where we model and investigate strong coupling to plasmonic nanowires arising from the corrugated back reflector. In Section 4 we optimize the structure and demonstrate that the absorptance in the entire device is 98%, with 92% being in the WSe_2 layer and nanowires, and 82% in the WSe_2 alone. We compare this to other architectures in Section 5 and demonstrate that our structure out-performs these alternatives by a wide margin. Thus, our proposed approach is a highly absorbing candidate for optoelectronic devices involving scalably grown 2D materials, beyond just the WSe_2 on which we focus in this work.

Our findings improve upon the existing designs in three ways. First, many works focus only on achieving zero reflectance or creating overall perfect absorbers [9,10,12,34], and thus cite only total device absorptance as a metric. The non-parasitic absorptance that contributes to carrier photogeneration thus remains unknown in these structures. Second, much past work on enhancing TMD absorptance utilizes TMDs that are thicker than a few-layers, up to and including those that can support waveguide modes [13,35]. While these structures can demonstrate perfect absorptance in the TMD material, the thickness prohibits the desirable electronic properties associated with 2D behavior. Third, many structures in the literature rely upon mechanically exfoliated flakes, restricting the scalability of the proposed devices. In contrast, our structure is designed using a Al_2O_3 superstrate, enabling CVD grown WSe_2 to be used without any need for transfer processes. This constraint precludes the use of enhancement mechanisms on both sides of the WSe_2, such as the approaches in [21–23,34,35], which are based on creating a plasmonic or Fabry-Perot cavity around the 2D material. Instead, the constraint of CVD growth requires any structured metallic enhancement layers to exist on only one side of the Al_2O_3.

2. Planar architectures and Fabry-Perot enhancement

In this section, we consider the planar architecture shown in Fig. 1(a) which utilizes interference effects for enhancement; designs incorporating plasmonic effects will be discussed in later sections. We employ a back reflector to utilize the zero-mode effect [6,7], and insert a spacer layer to achieve further enhancement via an FP cavity. We work with 5 layers of WSe_2 based on

Optical Materials EXPRESS

a tradeoff between thickness and desirable 2D effects. We take the thickness of each layer as 0.7 nm [36], so that 5 layers is d_{abs} = 3.5 nm. To enable CVD growth, one side of the WSe_2 must have a layer of Al_2O_3 thicker than any optical length scale. Thus, for the purposes of our design, we assume that one side of the WSe_2 has a half-infinite slab of Al_2O_3. On the other side, we place a thin lossless spacer layer of thickness d_{FP}, and then a half-infinite slab of metal. This assumption is justified as long as a device constructed in practice has a metallic layer several skin depths thick. Considering the later integration with plasmonics and the desire to enhance not only in the UV, but also at longer wavelengths [11], we use Au. In reality, the metallic back reflector need only be optically thick (several skin depths even for the lowest frequency) and not half-infinite. As for the lossless spacer, we use TiO_2 due to its high refractive index. This enables thinner plasmonic structures and thus larger aspect ratios, allowing better redshifting of the plasmonic resonance [37]. The material data for WSe_2 was taken from [38], where it is obtained ellipsometrically from a CVD grown sample atop sapphire. The optical material models for the other materials were obtained from [39–42].

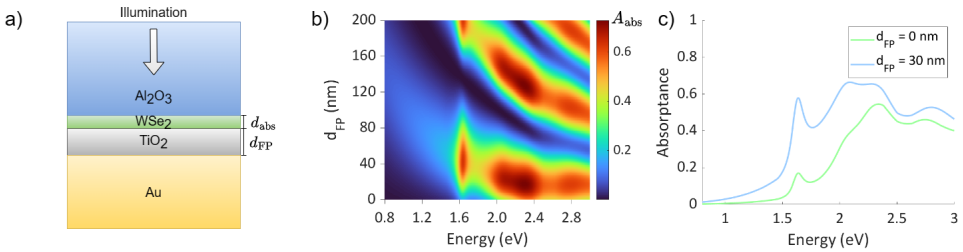

Fig. 1. Fabry-Perot cavity resonance-based enhancement of absorptance in the WSe_2. a) The planar layer structure consisting of an Al_2O_3 superstrate with few-layer WSe_2 below it, and a TiO_2 spacer and a Au back reflector. b) The absorptance spectra in only the WSe_2 layer as a function of photon energy and d_{FP}. c) Selected spectra from (b) depicting the case of no spacer (d_{FP} = 0 nm, green) and optimal TiO_2 thickness used in the rest of this work (d_{FP} = 30 nm, blue).

The absorptance in only the WSe_2 layer upon illumination through the Al_2O_3 is calculated as $A_{abs}(\omega) = 1 - R(\omega) - T(\omega)$, where ω is photon frequency, reflectance $R(\omega)$ is from the top surface of the WSe_2 and transmittance $T(\omega)$ is into the back reflector. The dependence of $A_{abs}(\omega)$ on d_{FP} and photon energy E, calculated via the Transfer Matrix Method (TMM), is shown in Fig. 1(b). Figure 1(c) depicts slices from this graph, illustrating the enhancement that can be obtained with the additional degree of freedom provided by the TiO_2 spacer. This enhancement stems from the increase of the electric field at the location of the absorbing TMD. The conventional shape of the FP fringes with $d_{FP} \propto \omega^{-1}$ dependence is observable in Fig. 1(b), modulated by the absorption of the TMD. We choose an optimal d_{FP} that contains as many absorption resonances as possible that coincide with FP fringes. This is easier to achieve when d_{FP} is small and the fringe profile is flatter, with the added benefit that it will be easier to achieve a high aspect-ratio nanowire for smaller d_{FP}, as previously discussed. Thus, we choose d_{FP} = 30 nm as the optimal thickness.

To analyze this structure, we note that the FP resonance is very broad at small d_{FP}, and one would observe a smaller period between FP peaks for larger thicknesses (due to the $1/d_{FP}$ dependence of thin film interference). The enhancement without visible hybridization (since the excitonic peak locations are roughly unchanged by increasing d_{FP}) implies that this is in the weak coupling regime, where the slab structure is responsible for increasing the field in the TMD. Essentially, we are coinciding a FP peak with the absorption peak of the WSe_2, so that the electric field strength is enhanced and more absorption occurs in the WSe_2. Moreover, the lowest order FP fringe is the flattest for the wavelength range of interest, and therefore enhancement can be observed for all peaks simultaneously. Thus, optimal weak coupling at all excitonic peaks

Optical Materials EXPRESS

of interest can be achieved by choosing a roughly optimal value such as d_{FP} = 30 nm, which we shall use for the rest of the analysis here. We note that the lowest FP fringe would be higher than that shown in Fig. 1(b) in the absence of a lossy material such as Au, which provides a phase change at the interface that decreases the required propagation length for interference. The lowering of this branch allows a selection of d_{FP} that simultaneously enhances a broad range of excitonic peaks, rather than the higher order fringes which are steeper and enhance different excitonic modes at different values of d_{FP}. In the presence of only lossless interfaces, reflection would be lowest for $\lambda/4 = n\,d_{FP}$, which, for $n = 2.4$ and $\lambda = 750$ nm, would occur at $d_{FP} = 78$ nm. Instead, the lossy back reflector and the resulting phase changes result in this phenomenon occurring at a lower d_{FP}.

To summarize, we have utilized a back reflector to take advantage of zero-mode enhancement (green line in Fig. 1(c)), and have further created a FP cavity to increase the absorptance (blue line) in a 2D TMD.

3. Analysis of anticrossing and spectral modeling for a corrugated back reflector

We next corrugate the back reflector (Au layer in Fig. 1(a)), such that a periodic array of plasmonic nanowires emerges. The nanowires are infinite in one direction, and the only tunable parameters are thus the width w, the height d_{pl}, and the period b. The localized plasmonic modes are excited by polarization perpendicular to the nanowires. We investigate the entire range of nanowire widths, from $w = 0$ to $w = b$. This range of structures is shown in Fig. 2(a). The $w = 0$ case is simply the FP spacer of the previous section, whereas the $w = b$ case is equivalent to the lack of any TiO_2 spacer. Situations close to $w = 0$ comprise a regular nanowire array, whereas situations close to $w = b$ are better described as the inverse of this, an array of trench lines etched in the Au. We do not consider an additional FP cavity atop the plasmonic structures to better take advantage of the near field enhancement. This constrains $d_{pl} = d_{FP}$. In this section, we work with a Lorentzian approximation (see Supplement 1) to simplify the modeling process and only consider a single excitonic peak (other excitonic peaks could be added if desired).

3.1. Width sweep

In this section, we sweep over the entire range of possible nanowire widths w from 0 to $b = 400$ nm and take $d_{FP} = d_{pl} = 30$ nm. The results are shown in Fig. 2. We use three power monitors in our simulations, which are conducted via the Finite Difference Time Domain (FDTD) Method [43]. The reflectance monitor, yielding $R(\omega)$, is placed at the interface of the WSe_2 and Al_2O_3; one transmittance monitor, yielding $T_{abs}(\omega)$ is placed at the interface of the WSe_2 and TiO_2, and another transmittance monitor is placed at the interface of the nanowire array and the back reflector, yielding $T_{tot}(\omega)$. The absorptance in the WSe_2 is calculated as $A_{abs}(\omega) = 1 - R(\omega) - T_{abs}(\omega)$, and the "total" absorptance, which only includes absorptance in the WSe_2 and the nanowires, but *not* the back reflector, is given as $A_{tot}(\omega) = 1 - R(\omega) - T_{tot}(\omega)$. The grand total absorptance is $1 - R(\omega)$, so this method does not omit any information about the optical power.

Starting with the case for which $w = 0$, we see that at low frequencies, most of the incident power is reflected, due to Au being a better conductor at long wavelengths, and also the cavity effects being less prominent for longer wavelengths. At higher frequencies, most of the light is transmitted into and absorbed in the back reflector since Au is no longer close to a perfect conductor in this frequency range. The spectra also demonstrates absorptance in the WSe_2 at its Lorentzian peak. Similar results can be seen for the $w = b$ case, where the back reflector is effectively moved upwards by d_{pl} and eliminates the FP cavity. Thus, the absorptance in this layer is quite strong at high frequencies as visible in A_{tot}, whereas reflection is lower. We observe that the absorptance peak due to the Lorentzian WSe_2 response is less prominent, owing to the lack of the FP cavity.

Optical Materials EXPRESS

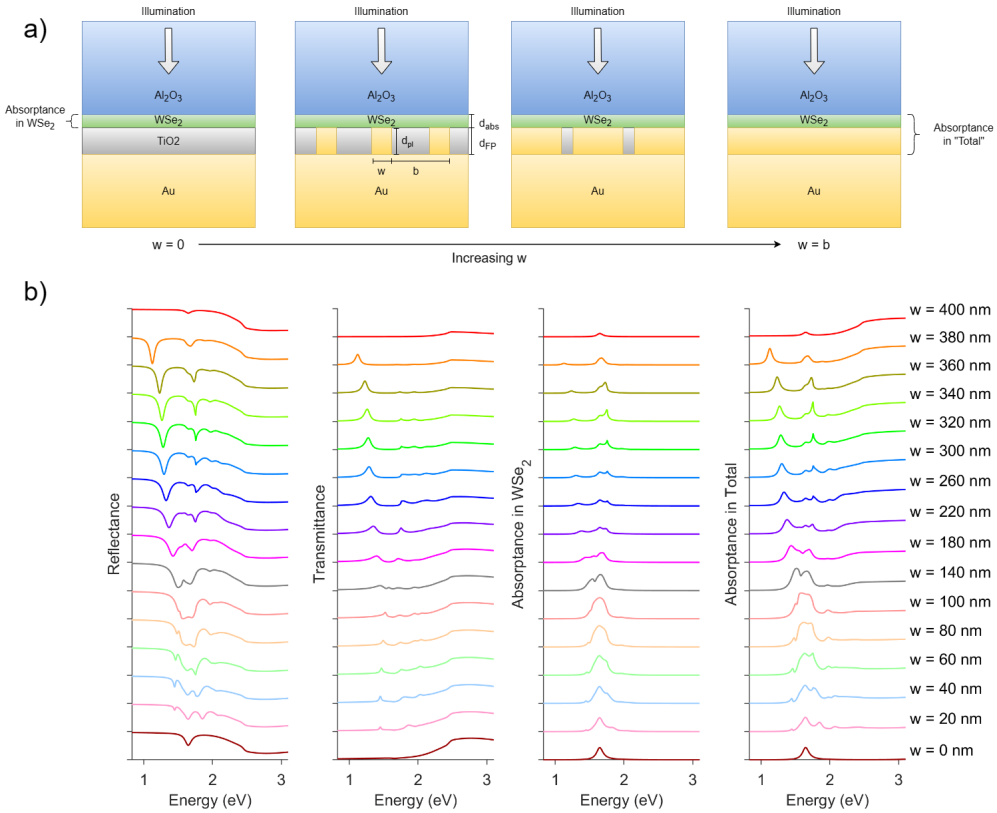

Fig. 2. a) Four of the nanowire widths w investigated in this paper. As w increases, there is a transition from a FP cavity to a nanowire back reflector, which becomes a gold mirror with slits in the back reflector as w increases, and ultimately becomes a back reflector without a FP cavity in the limit that $w = b = 400$ nm. b) Left to right: The reflectance, transmittance, absorptance in the WSe_2, and absorptance in the WSe_2 and plasmonic nanowire array ("total"). The spectra for the different values of w are offset for visibility.

For the lowest value of w tested for which the structure is non-planar ($w = 20$ nm), we observe 3 significant features in the spectra. There is the excitonic peak of WSe_2 at its usual position (1.65 eV), an LSPR peak near 1.84 eV, and an SPP peak at 1.45 eV. As w increases, we observe hybridization of these peaks. The physical origin of these peaks can be explained as follows. The peak at 1.65 eV is the excitonic resonance from our Lorentzian model of WSe_2. The peak at 1.8 eV for $w = 20$ nm strongly redshifts with increasing w, and the strength increases as well. We therefore conclude it is the localized surface plasmon. As for the SLR peak, we observe from Fig. 3(a) that the sharp resonant peaks redshift with increasing period. Further, observing Fig. 3(b), we see that the scattering pattern is consistent with an SPP formed by a diffractive effect due to the nanoantennae scattering transverse to the incident wavevector, forming a profile which decays away from the edge [44]. Moreover, the Fano resonant lineshape is in qualitative agreement with that expected for an SLR [45,46]. Justification for the quantitative locations of these peaks is discussed in the next subsection.

In the absence of hybridization (coupling) between these effects, the excitonic peak would be expected to remain constant as w changes. The LSPR peak would redshift due to the increased geometric dimension (along the electric field component exciting the plasmon) and associated increase in the effective optical "size" of the plasmonic structure, as well as the increase in aspect

Optical Materials EXPRESS

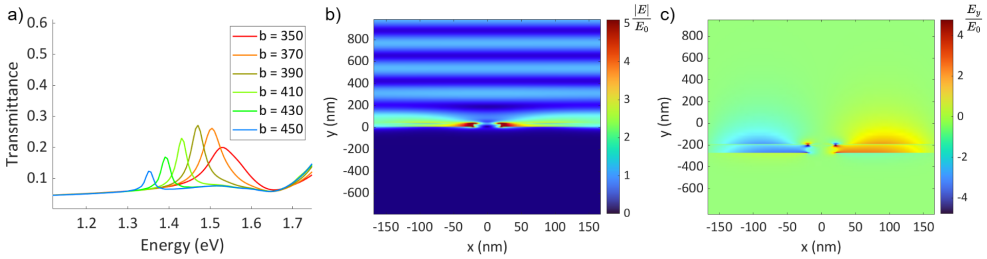

Fig. 3. a) Transmittance for variations in the period b of the nanowire grating at a width $w = 40$ nm. The sharp SLR peaks redshift with increasing period, as expected. b) The calculated electric field profile for $b = 350$ nm at 1.52 eV, where the SLR/SPP effect can be seen. c) The y component of the electric field, which is scattered for incident excitation with polarization along the x-direction. The color scale is truncated for small regions at the hotspots at the corners of the nanowires, which can have $|E|/E_0$ of upto 104.

ratio. The peak height would also increase due to the increasing geometry and the larger cross section of the nanowires at larger sizes. This overall behavior suggests that a separate description of the inverse structure etched into the back reflector is not necessary, and even for $w \approx b$, the conventional nanowire description holds for the most part. We can expect this optical behavior to break down if w gets even closer to b, as it reaches the limit of there being no plasmonic resonance at all. This is suggested by the fact that as w approaches b, the simulated LSPR peaks deviate from our analytical predictions made for a nanowire (see next subsection). Qualitatively, the sharp SLR peaks exist in two categories. For small w, we observe an SPP peak on the low energy side of the spectrum, starting at 1.45 eV in the transmittance spectra for $w = 20$ nm. A Fano resonance lineshape is observed in the reflectance and absorptance spectra. This shift can be attributed to the changing surrounding refractive index in which this diffraction and SPP formation occurs. For larger w, the SPP peak is barely visible after it crosses to the other side of the plasmon, in agreement with the results of [45].

In terms of the hybridized peak behavior seen in Fig. 2, we observe that the most prominent feature in the spectra is the anticrossing observed between the excitonic peak and the redshifting plasmonic peak. In the absence of coupling, these peaks would reach resonance and cross at a width of about $w = 80$ nm. When coupling occurs, the new eigenstates of the system become polaritons, more specifically so-called “plexcitons" in the case of mixing between plasmonic and excitonic modes [47]. The Rabi splitting between the polariton branches is thus $\sim$ 100 meV, as can be viewed in Fig. 2. We refine our prediction for this value in the next subsection. This value is higher than the majority of the values reported in the graph in [23] and the table in [35]. The highest of these values is also ~100 meV, only surpassed by the very strong coupling of $\sim$ 0.4 eV reported by the authors of the latter work. The value of $\sim$ 0.4 eV was achieved by patterning WS_2 into ellipses; however, these structures are bulk and not few-layer [35]. Furthermore, this anticrossing behavior is accompanied by hybridization with the SLR mode as it blueshifts for increasing w.

3.2. Hamiltonian analysis

We can analyze this anticrossing behavior via the diagonalization of a 3×3 Hamiltonian, written as [37,48]:

$$H = \begin{pmatrix} E_{0,1} - i\Gamma_1 & V_a & V_b \\ V_a & E_{\text{pl}} - i\Gamma_{\text{pl}} & V_c \\ V_b & V_c & E_{\text{SLR}} - i\Gamma_{\text{SLR}} \end{pmatrix} = SDS^{-1} \quad (1)$$

Optical Materials EXPRESS

where the diagonal contains the resonant energies of the system, accompanied by the decay coefficients associated with the imaginary parts making the matrix non-Hermitian. $E_{0,1} - i\Gamma_1$ corresponds to the exciton, $E_{\mathrm{pl}} - i\Gamma_{\mathrm{pl}}$ to the plasmon, and $E_{\mathrm{SLR}} - i\Gamma_{\mathrm{SLR}}$ to the SLR. The off-diagonal terms are coupling coefficients, which can be complex in general, but real values will suffice for our analysis. The diagonalized matrix D contains the hybridized energies E_m $(m = 1, 2, 3)$ on the diagonal, and the matrix of eigenvectors S contains the coefficients S_{ij} which are the contribution of the i^{th} mode to the j^{th} eigenstate of the system.

The values of the unhybridized resonances that enter H prior to diagonalization can be found as follows. The location of the LSPR is found by treating the nanowires as plasmonic dipoles, and the location of the SLR is found by diffractive coupling to an SPP mode. These methods are discussed further in the Supplement 1. The location of the excitonic resonance can be identified from the permittivity model used for WSe_2. We plot the hybridized models over the simulated spectra for $b = 350$ nm and $b = 400$ nm in Fig. 4.

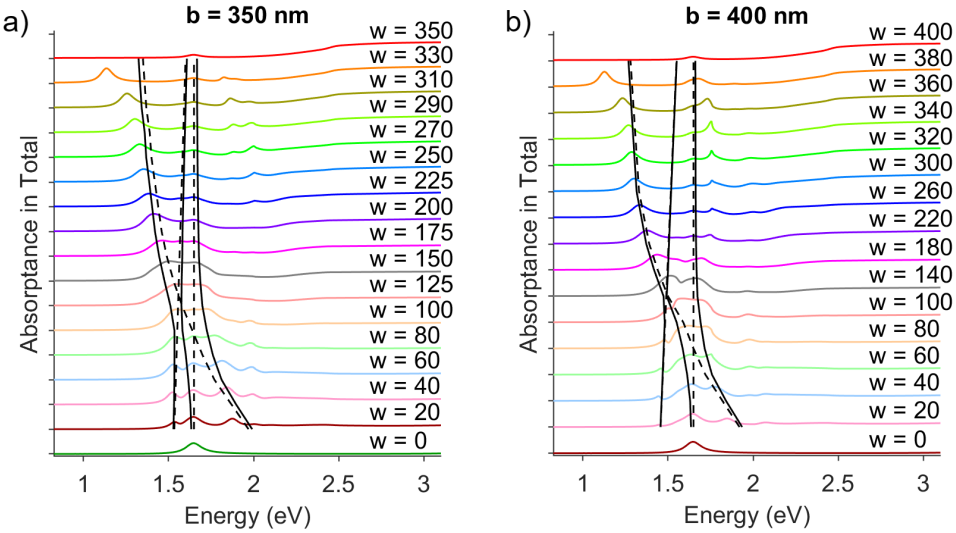

Fig. 4. Absorptance spectra for a range of nanowire widths and modeled modal coupling for a) $b = 350$ nm and b) $b = 400$ nm. Dashed black lines are predicted unhybridized mode locations, and solid black lines are the resulting hybridizations from our Hamiltonian model. Strong coupling with Rabi splittings of 150 meV (at $b = 350$ nm) and 130 meV (at $b = 400$ nm) are observed.

The Hamiltonian captures the essential behavior of the coupling between the WSe_2 resonance, the LSPR, and the SLR, as can be seen in Fig. 4. For $b = 350$ nm, we obtain $V_a = 75$ meV, $V_b = 0$ meV, and $V_c = 50$ meV. For $b = 400$ nm, we obtain $V_a = 65$ meV, $V_b = 0$ meV, and $V_c = 20$ meV. Thus, it is not necessary to account for direct coupling between the WSe_2 mode and the SLR: any coupling is mediated by the LSPR. The coupling between the LSPR and the WSe_2 mode implies a Rabi splitting of 150 meV and 130 meV for $b = 350$ nm and $b = 400$ nm, respectively, which is high compared to values in the literature [23]. It is also worth noting that the SLR is much more strongly visible on the low energy side of the LSPR, and much weaker on the other side. The former regime is well-described by a Fano phenomenon, but the latter is better described by a coupled dipole approximation, as described in [45]. Our results and lineshapes for the SLR are consistent with those found by the authors of [45]. We note that the deviation of the leftmost solid and dashed black lines (unhybridized and hybridized modes) in Fig. 4 from the simulated LSPR peak for large w is a result of the individual nanowire description breaking down at large w.

Optical Materials EXPRESS

To establish the strong exciton-LSPR coupling in our structure, we turn to the strong coupling criterion in [49]:

$$2V_a > \frac{\Gamma_1}{2} + \frac{\Gamma_{pl}}{2} \tag{2}$$

which states that the Rabi splitting should be sufficiently large compared to the individual peak widths. At the point of closest approach of the polariton ("plexciton") branches for 350 nm (at w = 100 nm), the value of the coupling strength is V_a = 75 meV, and the corresponding damping constants are Γ_1 = 100 meV and Γ_{pl} = 70 meV. Thus, strong coupling between the exciton and plasmon is clearly achieved, indicating that energy transfer between the modes will occur multiple times before the energy is dissipated. For b = 400 nm, there is yet again strong coupling, since at the point of closest approach of w = 80 nm, V_a = 65 meV, Γ_1 = 100 meV, and Γ_{pl} = 80 meV. However, if we apply a similar criterion to the coupling with the Fabry-Perot mode from Section 2, we see that the FP mode is very broad at d_{FP} = 30 nm, and there is barely any shift in the peak. Thus we can indeed conclude that this is weak coupling.

4. Optimal structure for absorption

Having investigated the model of a single excitonic peak and its interaction with plasmons and the lattice resonance, we now vary w to design a device incorporating the complete WSe_2 model from [38] in order to design a structure to achieve maximum absorption. The parameters we obtain are w = 80 nm, b = 400 nm, and $d_{FP} = d_{pl}$ = 30 nm. The period sweep shown in Fig. 3 also suggested that b = 400 nm was near optimal. The thickness of the FP cavity, d_{FP}, was chosen by optimizing across the enhancement of various peaks, as in Section 2. The results can be seen in Fig. 5. At the optimal value of w = 80 nm, the plasmonic peak coincides and undergoes coupling and anticrossing with the excitonic peak. This is the point of closest approach discussed in the previous section, and where the coupling is thus the strongest.

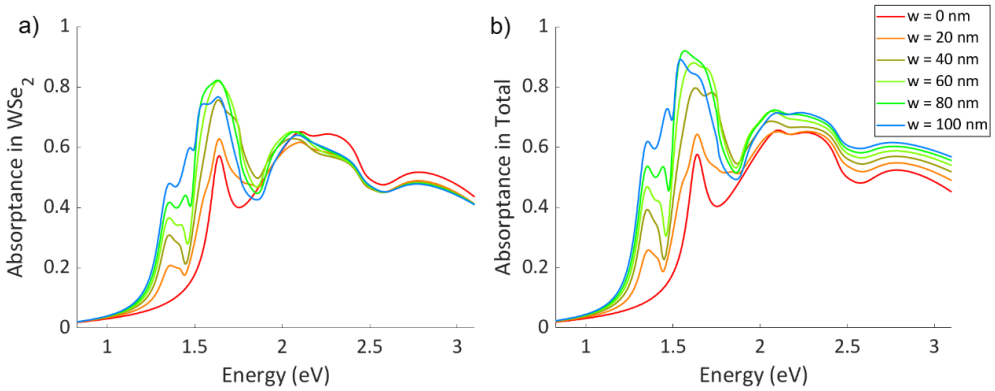

Fig. 5. The absorptance spectra as w is varied, for a structure incorporating the full WSe_2 model, with b = 400 nm, and d_{FP} = 30 nm. a) Absorptance only in the WSe_2. b) Absorptance in the WSe_2 and the plasmonic layer.

There are two peaks visible near the global maxima of the absorptance spectra in Fig. 5. A spectral dip arising from the interference of the SLR with the other resonances is visible near 1.4 eV, and the other excitonic peaks are visible at higher frequencies. We choose w = 80 nm as the optimal nanowire width since it demonstrates the highest peak absorptance both in WSe_2 alone (Fig. 5(a)) and in WSe_2 and the nanowires together (Fig. 5(b)), and also because it has large broadband absorptance. In summary, peak absorptance in the WSe_2 is 82% (1.64 eV), the total peak absorptance in the WSe_2 and the nanowires is 92% (1.56 eV), and the grand total peak

Optical Materials EXPRESS

absorptance (calculated as $1 - R$) is 98% (1.56 eV), achieving essentially a perfect absorber in the range 1.5-1.7 eV, with a large portion of the absorptance in the WSe_2.

5. Comparison of architectures

We now compare the structures we have investigated to a set of other possible architectures (shown in Fig. 6(a)) to assess our design. Our design space is constrained by the necessity for WSe_2 to be adjacent to the Al_2O_3 for CVD or other high-temperature growth to be possible, and thus negate the need for WSe_2 transfer processes. The transparent substrate enables enhancement mechanisms to be applied on either the top (the side from which light is incident) or the bottom of the structure. First, we consider the simplest case, in which we have the WSe_2 on an Al_2O_3 substrate, and the light is incident directly on the WSe_2 from free space. We then place a TiO_2 spacer on top of the WSe_2 to act as an antireflection coating with FP modes and further confine light into the TMD. Repeating a similar analysis as in Section 2, we determine $d_{FP} = 120$ nm as the optimal thickness. We then embed the 80 nm wide, 30 nm thick nanowire array with period 400 nm investigated in Section 4 into this TiO_2 layer. This group of structures (no TiO_2 or Au, TiO_2 only, and TiO_2 and Au), constituting the top row of Fig. 6(a), is labeled 1-3 in the figure. We then compare this to the cases in which Al_2O_3 is the superstrate, which enables the use of a back reflector. The first of these structures is simply the WSe_2 sandwiched between half-infinite slabs of Al_2O_3 and Au. Next, we insert a TiO_2 spacer between the WSe_2 and Au, forming an FP cavity, and then modify the Au to add the corrugated back reflector as discussed earlier. This can also be viewed as simply comparing the limiting cases $w = 0$, $w = b$, with the optimal value of $w = 80$ nm. We refer to these structures, occupying the bottom row of Fig. 6(a), by the labels 4-6 in the figure.

As can be seen in Fig. 6(b), the absorptance is limited for case 1 without any enhancement mechanisms. Even in the presence of a TiO_2 spacer for case 2, the results do not change significantly, since the zero-mode enhancement effect is absent without a back reflector. Thus, a spacer, which has the potential to enable anti-reflection, ends up increasing the trasmittance into the substrate rather than the absorptance in the WSe_2. In both cases, the peak absorptance is $\lesssim 0.3$. An array of nanowires (case 3) can create enhancement in this structure; however, the enhanced absorptance is still limited, partially due to the fact that plasmonics on the front surface of the structure "shadow" parts of the WSe_2, reducing absorption in those regions. The peak absorptance in this structure barely surpasses 40%, and only in a limited spectral region near 1.5 eV.

For the cases where the enhancement mechanism is due to structures applied below the WSe_2, we see that the simple addition of a back reflector for case 4 increases broadband absorptance drastically (to above 0.4) for the higher frequency peaks owing to the zero-mode effect, but the enhancement at the lowest energy excitonic peak is limited. Use of a FP cavity (case 5) can enhance absorption in this region as well, creating absorptance values ~ 0.5 across most of the spectrum. The corrugated nanowire array in case 6, (which can be interpreted as the intermediate configuration between the presence and absence of a spacer), exploits the LSPR effect to further increase absorptance in the vicinity of the plasmonic resonance, to a peak value of 0.82, accompanied by only minor reduction in absorptance in other spectral regions compared to the $w = b$ case. Finally, comparison with Fig. 6(c) reveals that the bulk of the absorptance is in the WSe_2, rather than parasitically in the nanowire array. The LSPR mode is successfully coupling to the excitonic modes and causing enhancement. In Fig. 6(d,e) we plot the enhancement in all of the architectures, relative to a planar film of WSe_2 grown atop an Al_2O_3 substrate (architecture 1). There is a broad enhancement peak that architecture 4 provides, consistent with the weakly coupled Fabry-Perot mode. The spectra for Architectures 3 and 6, which display LSPR resonances due to the nanowires, contain narrower but taller enhancement

Optical Materials EXPRESS

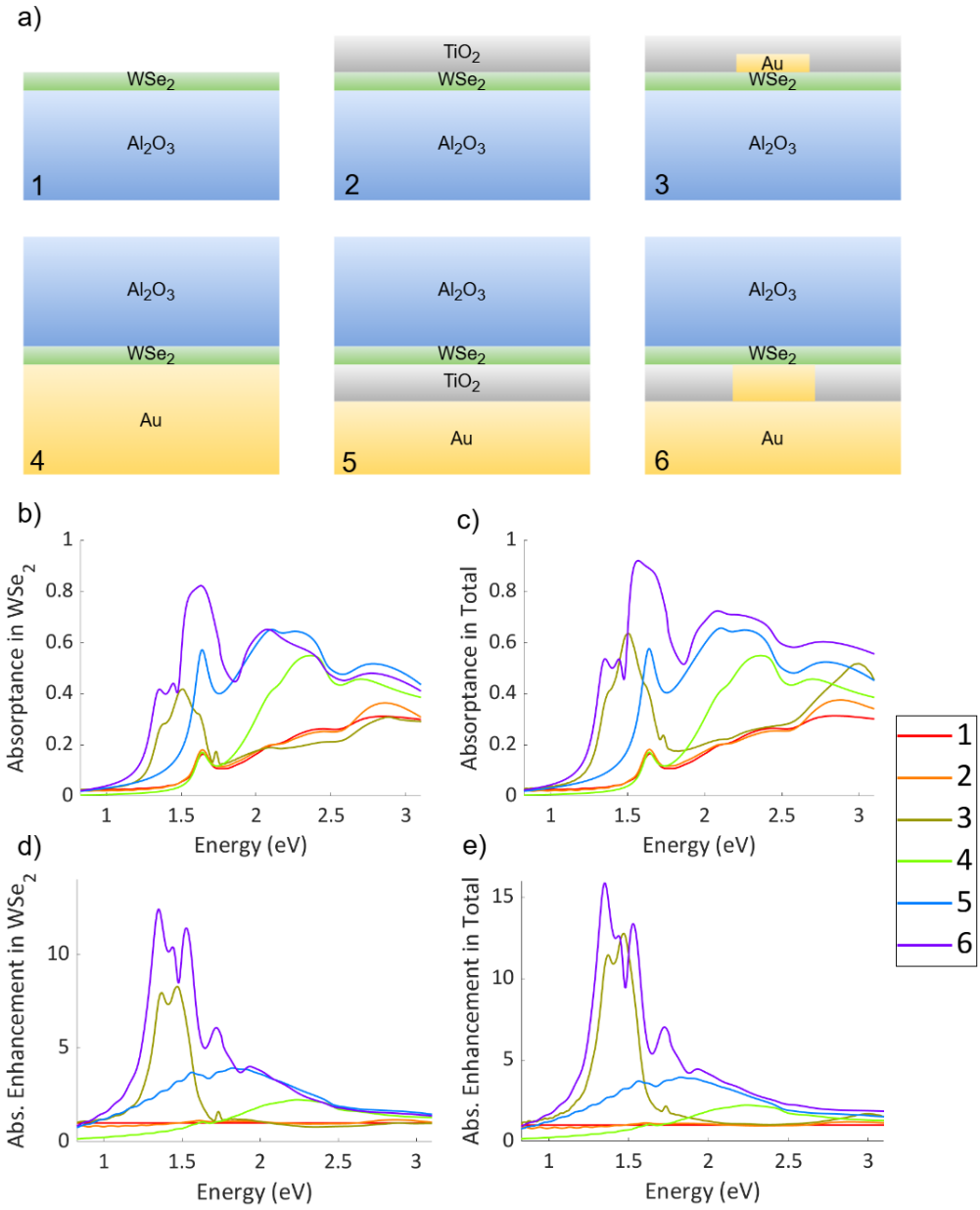

Fig. 6. Comparison of different WSe_2 enhancement architectures. Illumination in all devices is from the top. a) The top row corresponds to enhancement mechanisms applied on top of the WSe_2 with respect to the illumination, and the bottom row corresponds to enhancement mechanisms applied below the WSe_2. 1, 2, and 3 are the bare structure, addition of a TiO_2 antireflection layer, and addition of Au nanowires respectively; 4, 5, and 6 are the back reflector, addition of FP cavity enabled by a TiO_2 layer, and addition of nanowires, respectively. b) Absorptance in only the WSe_2 and c) absorptance in the WSe_2 and nanowire array (where applicable) for each of the 6 architectures shown in (a). d) Absorptance enhancement in the WSe_2, calculated relative to the absorptance of a planar film of WSe_2 on an Al_2O_3 substrate (red spectrum 1 in the legend), and e) enhancement of total absorptance relative to the planar film of WSe_2 on an Al_2O_3 substrate.

Optical Materials EXPRESS

features. Thus, our enhancement structure design is well-posed for optoelectronic applications in which the absorbing layer is WSe_2 or 2D materials with similar absorption profiles.

6. Conclusion

In this work, we have demonstrated the design and modelled the physics of few-layer WSe_2 below a Al_2O_3 superstrate, accompanied by a Au back reflector corrugated with nanowires. This study had the purpose of maximizing absorption in the WSe_2 in a structure that is compatible with scalable growth techniques for the 2D material. Our findings demonstrate peak absorptances of 82% in the WSe_2 alone, 92% in the WSe_2 plus nanowires, and 98% total absorptance ($1 - R$). Thus, we achieve a near-perfect absorber, with most of the absorption in the WSe_2, rather than parasitically in the Au. Moreover, the broadband absorptance is also high in the optimized structure, consistently >50% over most of the spectrum. Analyzing the different optical effects, we observe that the enhancement mechanisms are essentially threefold. First, there is the enhancement due to the back reflector, exploiting zero-mode enhancement. Second, this effect can be further improved by the weak coupling that a FP cavity provides. Third, for a corrugated array of nanowires etched out of the back reflector, we utilize a LSPR for targeted enhancement of an excitonic peak near the plasmonic resonance, yielding the high absorptance of 82% in the optimized structure. The LSPR and excitonic coupling is strong, with a Rabi splitting of 130 meV. Finally, we compare our proposed architecture to other designs that are possible under the scalable WSe_2 growth constraint. We conclude that for the 1D plasmonic structure proposed, this design is indeed the most highly absorbing.

Future work could consider other plasmonic designs rather than the simple 1D nanowire array in this work, which may be more challenging to fabricate but could yield higher enhancement with greater tunability arising from more degrees of freedom in the design space, such as with quasiperiodic structures [50]. We note that our current design could also be straightforwardly extended to other 2D materials of interest, or any optoelectronic thin absorbing material. Our demonstration of high absorptance in few-layer WSe_2 should enable the use of its desirable and tunable electronic properties that rely on its thinness, without sacrificing absorption in photodetectors and other optoelectronics, particularly thin or wearable devices.

Funding. National Science Foundation (ECCS-1846239); U.S. Department of Defense (W911NF2120213).

Acknowledgments. The authors would like to thank Elisa Antolin for an insightful discussion.

Disclosures. The authors declare no conflicts of interest.

Data availability. The data underlying the results presented in this paper are made available by the authors at [51].

Supplemental document. See Supplement 1 for supporting content.

References

1. S. M. Girvin and K. Yang, *Modern Condensed Matter Physics* (Cambridge University Press, 2019).
2. M. H. Lee and W. Wu, "2D materials for wearable energy harvesting," Adv. Mater. Technol. **7**(9), 2101623 (2022).
3. E. Antolin, S. A. Svatek, C. Bueno-Blanco, *et al.*, "MoS_2 solar cell with 120 nm-absorber and 3.8% AM1.5G efficiency," in *IEEE 49th Photovoltaics Specialists Conference (PVSC)*, (2022).
4. C. Bueno-Blanco, S. A. Svatek, and E. Antolin, "Optical absorption of MoS_2 based ultrathin solar cells," in *IEEE 49th Photovoltaics Specialists Conference (PVSC)*, (2022).
5. E. Antolin, S. A. Svatek, C. Bueno-Blanco, *et al.*, "Ultrathin solar cells based on quasi-2D materials," in *Physics, Simulation, and Photonic Engineering of Photovoltaic Devices XII*, (2023).
6. M. A. Kats, R. Blanchard, P. Genevet, *et al.*, "Nanometre optical coatings based on strong interference effects in highly absorbing media," Nat. Mater. **12**(1), 20–24 (2013).
7. J. M. Llorens, J. Buencuerpo, and P. A. Postigo, "Absorption features of the zero frequency mode in an ultra-thin slab," Appl. Phys. Lett. **105**(23), 231115 (2014).
8. J. M. Llorens, J. Buencuerpo, J. M. Ripalda, *et al.*, "Amplification of the zeroth order mode in ultra-thin layers," Journal of Green Engineering **5**(4), 71–82 (2016).

Optical Materials EXPRESS

9. A. Ghobadi, H. Hajian, B. Butun, *et al.*, "Strong light-matter interaction in lithography-free planar metamaterial perfect absorbers," ACS Photonics **5**(11), 4203–4221 (2018).
10. K. V. Sreekanth, P. Prabhathan, A. Chaturvedi, *et al.*, "Wide-angle tunable critical coupling in nanophotonic optical coatings with low-loss phase change material," Small **18**(28), 2202005 (2022).
11. C. Rockstuhl, S. Fahr, and F. Lederer, "Absorption enhancement in solar cells by localized plasmon polaritons," J. Appl. Phys. **104**(12), 123102 (2008).
12. G. Scuri, Y. Zhou, A. A. High, *et al.*, "Large excitonic reflectivity of monolayer $MoSe_2$ encapsulated in hexagonal boron nitride," Phys. Rev. Lett. **120**(3), 037402 (2018).
13. Y. Zhang, W. Liu, Z. Li, *et al.*, "Ultrathin polarization-insensitive wide-angle broadband near-perfect absorber in the visible regime based on few-layer MoS_2 films," Appl. Phys. Lett. **111**(11), 111109 (2017).
14. J. Wong, D. Jariwala, G. Tagliabue, *et al.*, "High photovoltaic quantum efficiency in ultrathin van der Waals heterostructures," ACS Nano **11**(7), 7230–7240 (2017).
15. D. Jariwala, A. R. Davoyan, G. Tagliabue, *et al.*, "Near-unity absorption in van der Waals semiconductors for ultrathin optoelectronics," Nano Lett. **16**(9), 5482–5487 (2016).
16. Y. Zhou, G. Scuri, J. Sung, *et al.*, "Controlling excitons in an atomically thin membrane with a mirror," Phys. Rev. Lett. **124**(2), 027401 (2020).
17. P. Back, S. Zeytinoglu, A. Ijaz, *et al.*, "Realization of an electrically tunable narrow-bandwidth atomically thin mirror using monolayer $MoSe_2$," Phys. Rev. Lett. **120**(3), 037401 (2018).
18. Z. Li, E. Palacios, S. Butun, *et al.*, "Omnidirectional, broadband light absorption using large-area, ultrathin lossy metallic film coatings," Sci. Rep. **5**(1), 15137 (2015).
19. V. E. Ferry, L. A. Sweatlock, D. Pacifici, *et al.*, "Plasmonic nanostructure design for efficient light coupling into solar cells," Nano Lett. **8**(12), 4391–4397 (2008).
20. H. Talebi and F. Emami, "High performance ultra-thin perovskite solar cell by surface plasmon polaritons and waveguide modes," Optics & Laser Technology **165**, 109552 (2023).
21. M. Stührenberg, B. Munkhbat, D. G. Baranov, *et al.*, "Strong light–matter coupling between plasmons in individual gold bi-pyramids and excitons in mono- and multilayer WSe_2," Nano Lett. **18**(9), 5938–5945 (2018).
22. Y. Luo, G. D. Shepard, J. V. Ardelean, *et al.*, "Deterministic coupling of site-controlled quantum emitters in monolayer WSe_2 to plasmonic nanocavities," Nat. Nanotechnol. **13**(12), 1137–1142 (2018).
23. M.-E. Kleemann, R. Chikkaraddy, E. M. Alexeev, *et al.*, "Strong-coupling of WSe_2 in ultra-compact plasmonic nanocavities at room temperature," Nat. Commun. **8**(1), 1296 (2017).
24. J. Miao, W. Hu, Y. Jing, *et al.*, "Surface plasmon-enhanced photodetection in few layer MoS_2 phototransistors with au nanostructure arrays," Small **11**(20), 2392–2398 (2015).
25. B. Lee, J. Park, G. H. Han, *et al.*, "Fano resonance and spectrally modified photoluminescence enhancement in monolayer MoS_2 integrated with plasmonic nanoantenna array," Nano Lett. **15**(5), 3646–3653 (2015).
26. H. S. Lee, M. S. Kim, Y. Jin, *et al.*, "Selective amplification of the primary exciton in a MoS_2 monolayer," Phys. Rev. Lett. **115**(22), 226801 (2015).
27. S. Butun, S. Tongay, and K. Aydin, "Enhanced light emission from large-area monolayer MoS_2 using plasmonic nanodisc arrays," Nano Lett. **15**(4), 2700–2704 (2015).
28. J. Guo, L. Lin, S. Li, *et al.*, "WSe_2 /MoS_2 van der waals heterostructures decorated with Au nanoparticles for broadband plasmonic photodetectors," ACS Appl. Nano Mater. **5**(1), 587–596 (2022).
29. V. Selamneni, H. Raghavan, A. Hazra, *et al.*, "MoS_2 / paper decorated with metal nanoparticles (Au, Pt, and Pd) based plasmonic-enhanced broadband (visible-NIR) flexible photodetectors," Adv. Mater. Interfaces **8**(6), 2001988 (2021).
30. S. Ghods and A. Esfandiar, "Plasmonic enhancement of photocurrent generation in two-dimensional heterostructure of WSe_2 /MoS_2," Nanotechnology **32**(32), 325203 (2021).
31. W. Chen, R. Liang, Y. Liu, *et al.*, "Surface plasmon-enhanced photodetection in $MoTe_2$ phototransistors with Au nanoparticles," Appl. Phys. Lett. **115**(14), 142102 (2019).
32. J. Guan, J.-E. Park, S. Deng, *et al.*, "Light–matter interactions in hybrid material metasurfaces," Chem. Rev. **122**(19), 15177–15203 (2022).
33. J. Li, J. Liu, Z. Guo, *et al.*, "Engineering plasmonic environments for 2D materials and 2D-based photodetectors," Molecules **27**(9), 2807 (2022).
34. Y. Yao, R. Shankar, M. A. Kats, *et al.*, "Electrically tunable metasurface perfect absorbers for ultrathin mid-infrared optical modulators," Nano Lett. **14**(11), 6526–6532 (2014).
35. P. Xie, Q. Ding, Z. Liang, *et al.*, "Cavity-assisted boosting of self-hybridization between excitons and photonic bound states in the continuum in multilayers of transition metal dichalcogenides," Phys. Rev. B **107**(7), 075415 (2023).
36. A. Krasnok, S. Lepeshov, and A. Alú, "Nanophotonics with 2D transition metal dichalcogenides [invited]," Opt. Express **26**(12), 15972–15994 (2018).
37. C. Bauer, "Optical properties of aperiodic metallic photonic crystal structures," Ph.D. thesis, Physical Institute, University of Stuttgart (2013).
38. H. Gu, B. Song, M. Fang, *et al.*, "Layer-dependent dielectric and optical properties of centimeter-scale 2D WSe_2: evolution from a single layer to few layers," Nanoscale **11**(47), 22762–22771 (2019).
39. P. B. Johnson and R. W. Christy, "Optical constants of the noble metals," Phys. Rev. B **6**(12), 4370–4379 (1972).

Optical Materials EXPRESS

40. I. H. Malitson, "Refraction and dispersion of synthetic sapphire," Journal of the Optical Society America **52**(12), 1377–1379 (1962).
41. S. V. Zhukovsky, A. Andryieuski, O. Takayama, *et al.*, "Experimental demonstration of effective medium approximation breakdown in deeply subwavelength all-dielectric multilayers," Phys. Rev. Lett. **115**(17), 177402 (2015).
42. M. N. Polyanskiy, "Refractive index database," https://refractiveindex.info.
43. "Ansys Lumerical FDTD," https://www.ansys.com/products/optics/fdtd.
44. S. A. Maier, *Plasmonics Fundamentals and Applications* (Springer, 2007).
45. A. I. Väkeväinen, R. J. Moerland, H. T. Rekola, *et al.*, "Plasmonic surface lattice resonances at the strong coupling regime," Nano Lett. **14**(4), 1721–1727 (2014).
46. Z. Li, S. Butun, and K. Aydin, "Ultranarrow band absorbers based on surface lattice resonances in nanostructured metal surfaces," ACS Nano **8**(8), 8242–8248 (2014).
47. D. N. Basov, A. Asenjo-Garcia, P. J. Schuck, *et al.*, "Polariton panorama," Nanophotonics **10**(1), 549–577 (2021).
48. A. Christ, S. G. Tikhodeev, N. A. Gippius, *et al.*, "Waveguide-plasmon polaritons: Strong coupling of photonic and electronic resonances in a metallic photonic crystal slab," Phys. Rev. Lett. **91**(18), 183901 (2003).
49. P. Törmä and W. L. Barnes, "Strong coupling between surface plasmon polaritons and emitters: a review," Reports on Progress on Physics **78**(1), 013901 (2015).
50. P. Postigo and J. Llorens, "Optical absorption enhancement by photonic quasicrystals in thin films for photovoltaic applications," in *ICTON*, (2013).
51. E. G. Ozaktas, "Design of near-perfect absorptance in few-layer WSe_2 via cooperative enhancement mechanisms: data," Github, 2024, https://github.com/jhu-nanoenergy/Near-Perfect-Absorptance-TMDs .